

The symbiotic stellar system R Aqr: mm-wave imaging of the WD – AGB wind interaction

V. Bujarrabal*

Observatorio Astronómico Nacional (OAN/IGN)

E-mail: v.bujarrabal@oan.es

J. Alcolea

Observatorio Astronómico Nacional (OAN/IGN)

E-mail: j.alcolea@oan.es

J. Mikołajewska

Nicolaus Copernicus Astronomical Center (NCAC)

E-mail: mikolaj@camk.edu.pl

A. Castro-Carrizo

Institut de Radioastronomie Millimétrique (IRAM)

E-mail: ccarrizo@iram.fr

We have observed the symbiotic stellar system R Aqr. We obtained high-resolution ALMA maps of the 0.9 mm continuum distribution, the $^{12}\text{CO } J=3-2$ line, and some other molecular lines in R Aqr. The maps, which have resolutions ranging between 150 milliarcsecond (mas) and less than 20 mas, probe the circumstellar regions down to suborbital scales and directly image the gravitational interaction between the white dwarf (WD) and the wind from the Mira star. The AGB star was identified in our maps from the continuum and molecular line data, and we estimated the probable position of the secondary from a new estimation of the orbital parameters. Our radiocontinuum maps show the very inner regions of the nascent bipolar jets, down to scales of some AU. Continuum maps obtained with the highest resolution identify the AGB photospheric emission, a clump that very probably corresponds to the emission of the ionized surroundings of the WD, and a bridge of dusty material joining both stars, which is likely material flowing from the AGB primary to the WD secondary. Our maps of the $^{12}\text{CO } J=3-2$ line show a strong focusing in the equatorial plane of the wind beyond the orbit, which is composed of two extended plumes and a central strong condensation. We also present unpublished compact-array maps that identify some weak clumps and show that this source shows no significant extended emission of CO. The structure and kinematics of the different components very probably correspond to the expected spiral-like structure due to the interaction. We have developed a very simple heuristic model, based on general ideas from models of the hydrodynamics and chemistry in these objects, whose predictions are surprisingly comparable to the observations and serve to describe the main properties of the circumstellar shells at a scale of a few orbital diameters.

The Golden Age of Cataclysmic Variables and Related Objects V (GOLDEN2019)

2-7 September 2019

Palermo, Italy

*Speaker.

1. Introduction

Symbiotic stellar systems (SSs) are interacting binaries in which copious mass transfer is taking place between an evolved cool giant and a compact companion, usually an AGB star and a white dwarf (WD). The result of that interaction is the ejection of equatorial flows and fast bipolar jets. The relevance in the SS activity of the gravitational interaction between the wind from the primary and the compact secondary is stressed in recent 3D simulations, see [1, 2, 3, etc]. The resulting outflows are strongly focused toward the orbital plane and show simple or double spiral structure.

R Aqr is the best studied SS [4, 5, 6, and references therein]. The primary is a bright Mira-type variable and the companion is a WD. The two-arcminute-wide nebula is composed of an equatorial structure elongated in the east-west direction and a precessing jet. The orbital period of the binary system is long, ~ 43.6 yr, and the orbital plane is roughly perpendicular to the plane of the sky and projected in the east-west direction [4]. Recent Very Large Telescope (VLT) imaging [7] resolved both stars, which were found to be separated by ~ 45 milliarcseconds (mas). The photospheric diameter of the AGB star is ~ 10 -20 mas, from IR interferometry. Although molecular lines are very rarely detected in SSs, R Aqr is relatively well studied in molecular emission, including lines of SiO, H₂O, and CO [5, 6]. Parallax measurements from SiO Very Long Baseline Interferometry data indicate a distance of 218 pc, although the distance from the GAIA parallax is 320 pc; the origin of such a discrepancy is unknown, both measurements being subject to uncertainties.

2. ALMA observations

Observations at $\lambda = 0.9$ mm were performed with ALMA in November 2017. The resulting maps show half-power beam widths (HPBW) $\sim 40 \times 35$ mas, see Figs. 1 and 3. To better investigate the compact continuum clump, we also produced images of less sensitivity but higher spatial resolution by favoring long baselines, reaching a resolution ~ 10 mas thanks to the very high S/N ratio (~ 1000); see red contours in Fig. 1 and [6] for technical details.

We also present unpublished maps obtained in November 2018 with a more compact configuration, which yielded lower resolution ($0''.15$) and higher sensitivity. Some weak outer clumps were detected, Fig. 4. Details on the data reduction will be presented in a forthcoming paper.

3. Results

We detected continuum emission and several molecular lines from R Aqr. As mentioned, continuum maps were obtained weighting the visibilities in two different ways, to obtain resolutions between 30×40 and 10 mas. All our maps are centered on the continuum centroid (ICRS coordinates R.A.: 23:43:49.4962, dec.: $-15:17:04.72$), to which the offsets given here always refer. The maximum in the high-resolution continuum map is placed (with respect to the centroid) at $\Delta(\text{R.A.}) = +8$ and $\Delta(\text{dec}) = -0.4$ mas. As we see in the following, that maximum is expected to represent the Mira position. We expect absolute errors ~ 3 mas [6], which are enough for our purposes.

We detected several molecular lines: the intense ¹²CO and ¹³CO $\nu=0$ $J=3-2$ and weaker lines, including vibrationally excited lines and ²⁹SiO $\nu=0$ $J=8-7$. The ²⁹SiO $\nu=0$ line shows blueshifted absorption against the stellar continuum (in the range between -8 and -15 km s⁻¹ LSR), very probably owing to infalling gas in front of the star. The high-excitation ($\nu > 0$) lines and the absorption

feature show compact, barely resolved distributions. In Table 1, we give the main properties of those lines, which are necessary to identify the AGB star (Sect. 3.2). Only the $\nu=0$ ^{12}CO line shows a significant extent $\gtrsim 0''.5$ (Sect. 3.3). From comparison with low-resolution data, we deduce that a moderate amount of flux of $\sim 20\%$ is lost in our maps of $^{12}\text{CO } \nu=0 J=3-2$.

We also show new, unpublished maps of $^{12}\text{CO } J=3-2$ obtained with a more compact ALMA configuration, yielding a final resolution of $0''.17 \times 0''.14$. The S/N ratio is very high, ~ 300 , allowing the detection of very weak components (Sect. 3.3). Practically all flux is recovered in these maps.

3.1 Radiocontinuum

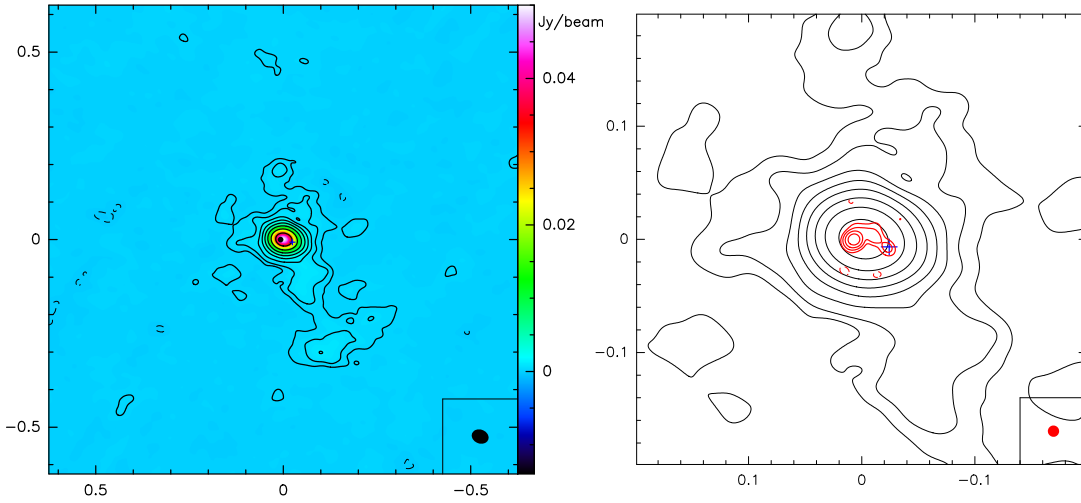


Figure 1: *Left:* ALMA map of the 0.9 mm continuum in R Aqr. The level spacing is logarithmic, with a jump of a factor 2. The map center is the continuum centroid and the positions of the two stars are indicated. See the HPBW in the inset. *Right:* High-resolution continuum map obtained using a 10 mas restoring beam, red contours. The scale is logarithmic: the first contour is 1.5 mJy/beam and the jump is a factor 2. The expected position of the WD is shown with error bars (blue cross) and the Mira is coincident with the maximum of the high-resolution map. See more details in [6].

Our 0.9 mm continuum maps are shown in Fig. 1, note the very high dynamic range. The positions of both stars are also given in Fig. 1, the AGB primary is represented by the black dot, whose width is roughly equal to the photospheric disk, and the blue cross gives the position of the WD; the stellar locations and the orbit are discussed in the next subsection and [6]. The main continuum component is very compact and elongated in the direction of the orbit. The low-brightness component is very probably the base of the bipolar jets (Sect. 1), detected down to scales of just some AU. The total flux is ~ 100 mJy, of which ~ 70 mJy comes from the central condensation, not much larger than the flux expected from the primary photosphere, ~ 35 mJy.

To better show the structure of the central continuum, we performed additional higher resolution maps by favoring long baselines; see results in Figs. 1 (*right*) and 2 and detailed discussion in [6]. This procedure yields a significant amount of lost flux and the jet is resolved out. The intense compact emission is shown to be composed of three components, identified in Fig. 2 as A, B, and C, from left to right. They show peak (total) fluxes of 23 (31), 6 (10) and 5 mJy beam $^{-1}$ (5 mJy), respectively. Comparing the fluxes in different subbands, we estimated the spectral index, finding

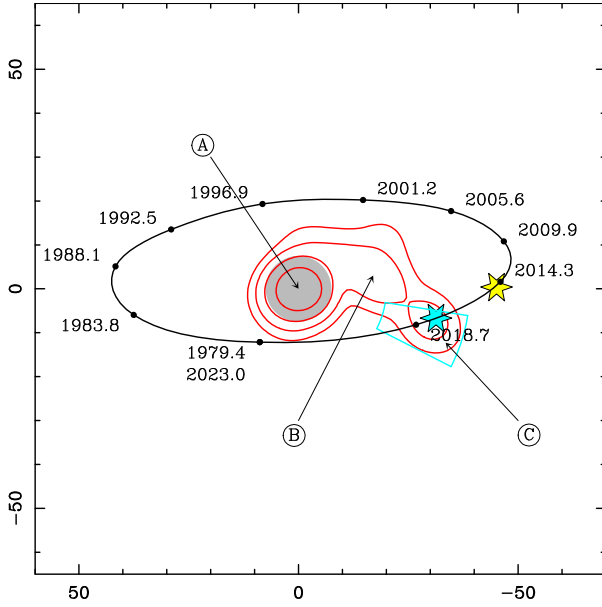


Figure 2: Main components (A, B and C) in our high-resolution continuum maps, red contours, and relative movement of both stars (mas), in gray, according to the new orbital parameters. The AGB star is represented by the gray circle (with a diameter of 15 mas), the position of the WD in [7, epoch 2014.9] is indicated by the yellow asterisk, and the position of the WD derived from the new orbital parameters for the epoch of our observations (2017.9) is indicated by the blue asterisk. The uncertainties are represented by the blue contour. Small black dots show the position of the WD at different orbital phases. See [6].

values of about 1.9, 3.1, and 1.0, respectively. Component A is coincident in position with the emission from vibrationally excited lines and the absorption feature of ^{29}SiO (Sect. 3.2), suggesting that this is indeed the emission from the Mira. Its total flux (31 mJy) and peak brightness are compatible with those expected from the Mira and its spectral index strongly suggests optically thick photospheric emission. We estimated the position of the WD companion for the epoch of our ALMA observations (2017.9), see Sect. 3.2, which is found to be coincident with our C component within the errors. This coincidence and the measured spectral index, which is compatible with emission from ionized gas around the WD, strongly suggest that this emission points to the location of the companion. The intermediate component B, which shows a spectral index compatible with dust emission, would be the first detection of mass transfer between the stars in a SS. We think that we are actually detecting both stars (or emission coming from their close surroundings) and the transfer of material from the primary to the secondary.

3.2 Position of the binary system

The high-excitation lines detected in our data are expected to come from the close surroundings of the AGB star and to be good tracers of its position, as well as the absorption in the $^{29}\text{SiO } \nu=0$ $J=8-7$ line [6, and references therein]. All these features show indeed compact images, whose centroids are practically coincident within the uncertainties, see Table 1. Their positions are also coincident with the continuum peak detected with the highest resolution (Sect. 3.1), particularly for the ^{29}SiO absorption. The differences are significantly smaller than the expected diameter of

Table 1: Main line parameters derived for high-excitation lines and ^{29}SiO absorption. We always give the R.A. and dec. offsets with respect to the total continuum centroid: 23:43:49.4962, $-15:17:0.4.72$.

molecular line	total flux mJy \times km/s	peak brightness mJy/beam \times km/s	Δ (R.A.) mas	Δ (dec) mas
$\text{H}_2\text{O } \nu_2=2 \ 3(2,1)-4(1,4)$	370 ± 15	174 ± 7	11 ± 3	3 ± 3
$\text{Si}^{17}\text{O } \nu=1 \ J=8-7$	100 ± 6	53 ± 4	10 ± 3	2 ± 3
$\text{CO } \nu=1 \ J=3-2$	310 ± 7	132 ± 5	11 ± 3	3 ± 3
$^{29}\text{SiO } \nu=0 \ J=8-7$ (abs.)	-53 ± 4	-48 ± 4	9 ± 4	0 ± 4
$\text{SO } ^3\Sigma \ \nu=1 \ 9(8)-8(7)$	307 ± 8	130 ± 5	14 ± 3	5 ± 3

the star, ~ 10 -20 mas. In any case, the line emission centroids tend to be shifted by about +3 mas in R.A. with respect to the position obtained from the continuum (Sect. 3.1). See discussion in [6]. We therefore conclude that the continuum peak position, namely ICRS R.A. 23:43:49.49657, dec. $-15:17:04.7204$, gives the AGB photosphere centroid with an accuracy of ± 3 mas. We have checked that these coordinates are fully compatible with the GAIA DR2 data.

The two stars were imaged in 2014.9 [7]. We estimated the evolution of the relative positions by adapting previous orbital parameters [4] to that measurement. See details on the orbit parameters in [6]; we plan to widely discuss them in a future paper. Our conclusion is that in 2017.9 the secondary was placed at about -31 mas in R.A. and -7 mas in declination, with respect to the Mira star, with an uncertainty of about ± 7 mas. We recall that the secondary is approaching us. The positions of both stars are given in some of our figures and the relative orbit is shown in Fig. 2.

3.3 $^{12}\text{CO } J=3-2$ maps

$^{12}\text{CO } J=3-2$ is the only line that shows a significant extent in our maps, see Fig. 3 and [6]. There is a compact central component plus two plumes at relatively negative and positive velocities, extending to the west and north-east, respectively, and occupying in total $\sim 0''.7$ (~ 200 AU).

The CO structure, clearly elongated in the direction of the projected orbit, obviously corresponds to mass ejection strongly focused in the orbital plane and the spiral-like pattern expected in our case from models, Sects. 1, 4. Up to a R.A. offset of $-0''.2$, the plume shows a slightly curved shape with concavity pointing northward, which is the expected projected shape of the inner spiral arm that is now being pushed by the companion. The outer clump at offset $\sim -0''.3$ seems to represent the second spiral arm, which must also move toward us. Finally, emission at relatively positive velocities (between -18 and -8 km s^{-1} LSR, Fig. 3) mostly comes from gas placed eastward and northward, as expected for an arm placed behind the star that, therefore, moves away from us.

We also show new, unpublished maps obtained with a more compact ALMA configuration, see Fig. 4 (note the different scale than in Fig. 3). The angular resolutions is $0''.17 \times 0''.14$. These data recover almost all flux and show a very high S/N (Sect. 2), allowing the detection of very weak components. The sparse compact clumps we see at distances of about $0''.5 - 1''$ represent all the (very weak) extended emission from R Aqr. The central intense component extending $\sim 0''.3$ is that shown in Fig. 3 with more detail.

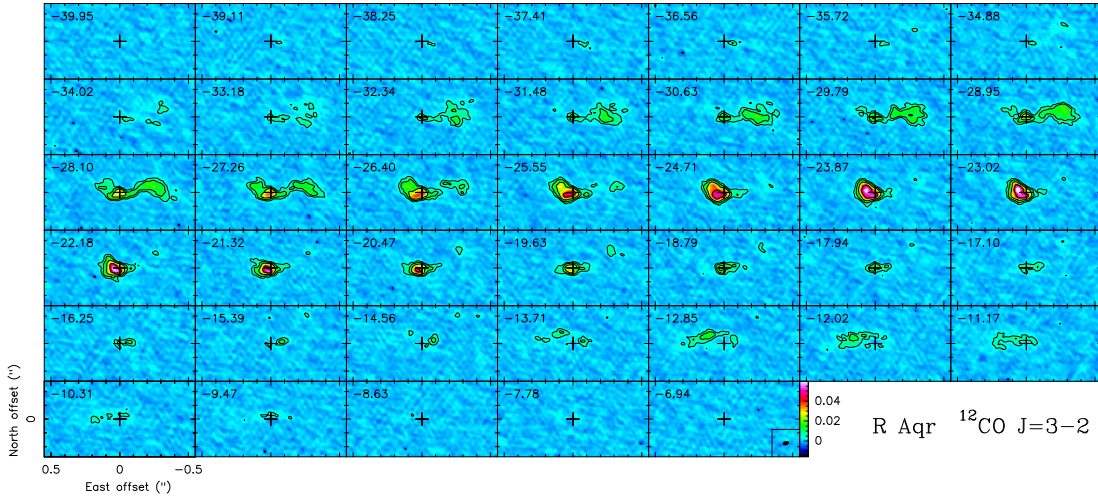


Figure 3: ALMA maps per velocity channel of $^{12}\text{CO } J=3-2$ emission in R Aqr; see the *LSR* velocities in the upper left corners. The center is the centroid of the continuum, whose image has been subtracted. The contours are logarithmic with a jump of a factor 2. See the HPBW in the last panel and [6] for more details.

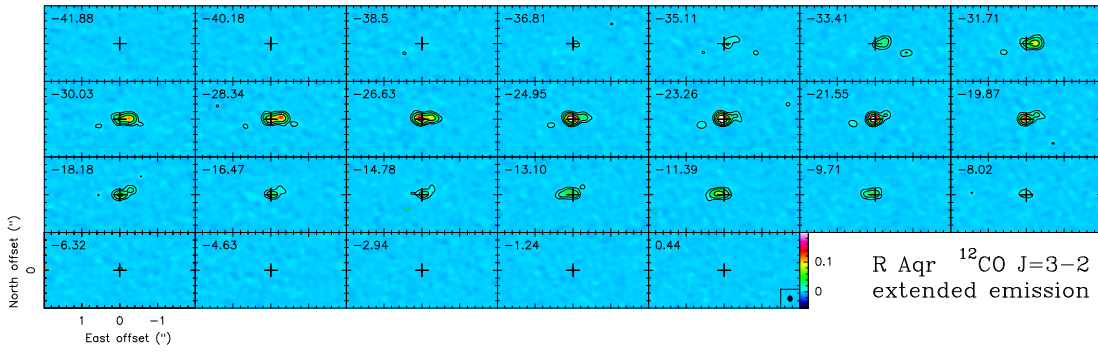


Figure 4: ALMA maps per velocity channel of $^{12}\text{CO } J=3-2$ emission in R Aqr obtained with a more compact configuration; see the *LSR* velocities in the upper left corners. The center is the centroid of the continuum, whose image has been subtracted. The contours are logarithmic, the first one is ± 6 mJy/beam (equivalent to 4.1 times the rms and 2.5 K) and the jump is of a factor 3. Note the high S/N ratio: all the weak features at a distance of about 1" are real detections. The HPBW is shown in the inset, last panel.

4. A simple heuristic model of the CO-rich envelope around R Aqr

We have tried to reproduce our maps using predictions of hydrodynamical models and of gravitational interaction between the AGB wind and the WD (Sect. 1), as well as simulations of expected line emission from the resulting gas distribution. We can reach a vaguely qualitative agreement, but, in general, the results are not satisfactory. First of all, the contrast between arms and interarm regions and between equatorial and adjacent regions is strongly underestimated in the simulations. The total extent of the emitting region is also too large, with an overall size more similar to those of standard AGB stars than to the tiny extent found in R Aqr.

It seems that a simple estimate of the emission using the gas density, temperature, and velocity distributions predicted by hydrodynamical models cannot lead to brightness distributions similar to

those observed. In addition, any attempt to iterate, using both hydrodynamical and line emission simulations and comparing the results with the data, is very slow and becomes soon too painful, because of the long and delicate calculations required.

The first problem is the molecule photodissociation by the UV radiation of the WD, which can be very intense at these short distances [8, 9, and references therein]. Photodissociation rates as short as 1 s^{-1} can be expected in inner shells. Molecules can only survive in regions where selfshielding and shielding by dust are very strong, at least in the dense shells very close to the AGB. For very abundant molecules like CO, selfshielding is the dominant effect. On the other hand, the formation of molecules can also be fast in the densest shells [10], in which we can expect competing formation and dissociation reactions with typical times of about one year. These time scales are very short, particularly in comparison with the orbital period of the system, 44 yr. Therefore, we can expect that most molecules are only abundant in a very small region at a few stellar radii from the AGB star. Since the shadow of the AGB star itself is important, such a molecule-rich region will extend mostly behind it, and, since the chemical time scales are very short, we can expect an elongated molecule-rich region evolving almost in phase with the stellar orbit. Only for very abundant molecules, like ^{12}CO , a relatively extended distribution is possible, well beyond the orbit. These general considerations are confirmed by our observations (Sect. 3). However, detailed calculations of the chemistry under these conditions of very complex geometry and fast evolution are extremely difficult.

Calculations of the expected emission from molecule density distributions deduced from hydrodynamical and chemical models are, therefore, of a great complexity. Instead, we have developed a simple heuristic approach, consisting in the definition of spiral like structures, based on general ideas derived from hydrodynamical calculations, and assuming that CO is only abundant in certain dense regions and practically absent elsewhere. We will try in this way to derive the properties (shape, density, temperature, and velocity field) that the actual distribution of the CO-rich gas must satisfy to be compatible with observations. Although, of course, not all the parameters can be accurately determined, some of the main ones can be derived or at least constrained. For such a purpose, we first assume a 3D spiral-like structure, including distributions of density and temperature and the velocity field. Then, we calculate the expected emission maps, after convolving the synthetic brightness distribution with the ALMA beam, and with the same format and units as the maps. Our code is similar to that described and discussed in previous works, see [11] for instance. The comparison of predicted and observed maps suggests changes in the model nebula, with which new predictions are obtained and a new comparison. The iteration is relatively fast, because the calculations do not require a significant amount of computer time and the necessary changes are quite directly suggested by previous comparisons.

In Fig. 5 we show the predictions of a preliminary fitting of our maps of $^{12}\text{CO } J=3-2$ (Fig. 3), the units and scales are the same and both figures are directly comparable. We see that the fitting is reasonably good. Fig. 6 shows the density distribution in the plane of the equator (*left*) and in a direction perpendicular to it (*middle*, $y=0$ plane). We stress that the density values refer only to the CO-rich gas and strongly depend on the very uncertain CO abundance.. We see the clear spiral structure and the high contrast between the CO-rich and photodissociated regions. As discussed, both properties are expected from theoretical considerations.

The interpretation of the meaning of the different components is straightforward. **A** is the

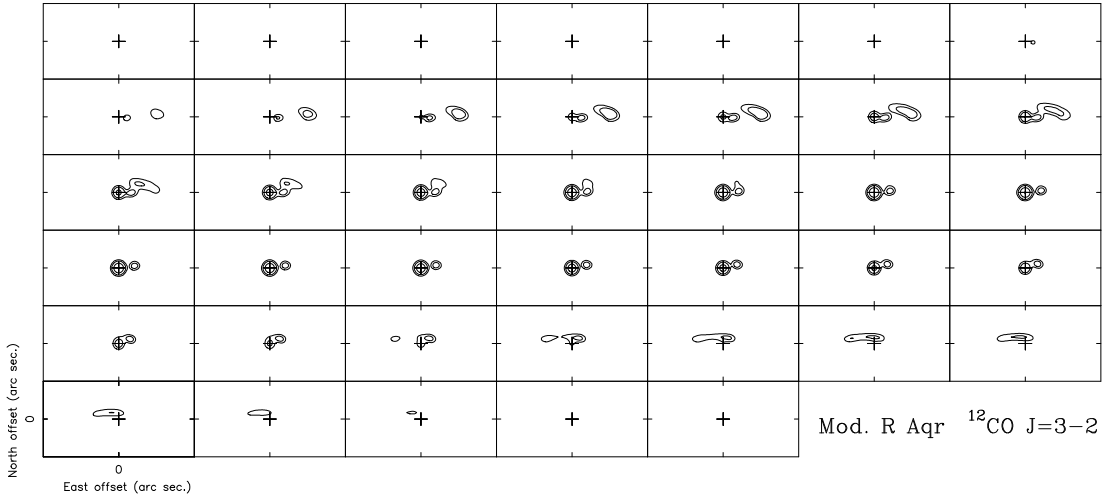


Figure 5: predictions of our simple heuristic model, to be directly compared with Fig. 3. Contours and units are the same as in that figure. We can see that the predictions are reasonably similar to the observations.

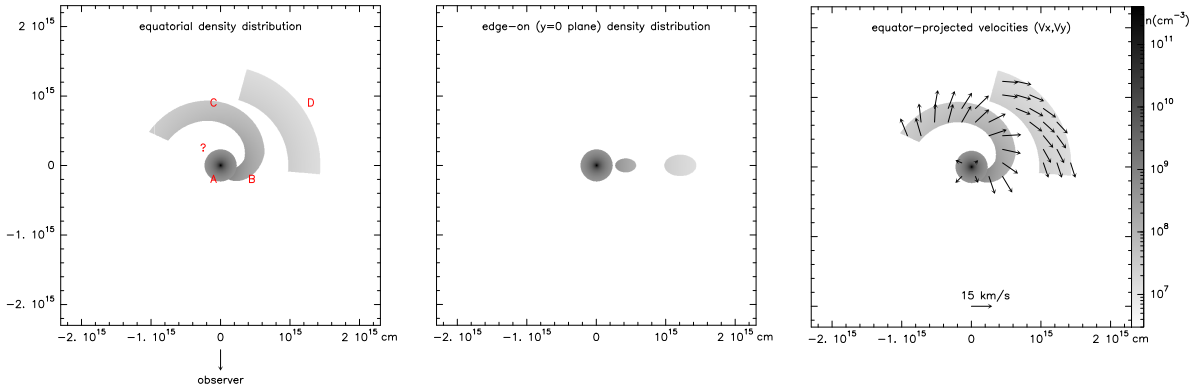


Figure 6: Density distribution of the CO-rich gas in our preliminary heuristic model *Left:* Density distribution in the equatorial plane. *Middle:* Density distribution in a plane perpendicular to the equator ($y=0$ plane). *Right:* Tentative velocity field.

central condensation, very close to the AGB star, where molecules are still abundant because of the high densities and shielding. **B** and **C** are the first spiral arm, directly dragged by the orbital movement of the WD. In our case, the orbit proceeds clockwise (as shown by measurements of the AGB velocity) and the circumstellar gas, which originally was in expansion, is entrained in that direction. **D** is a second arc, it could be the continuation of the first one or maybe the outer part of a second arm (often predicted by calculations). In these components, we expect some combination of expansion and rotation, i.e. radial and tangential velocity; velocity moduli between 10 and 15 km s^{-1} are required (Fig 6, *right*). Note that the modeling of the velocity field is particularly uncertain because we only have information on the projection on the line of sight. There is another component, **?**, of uncertain origin and in fact not included in our nebula model, see discussion below.

The model components from which the observed features come are shown in Fig. 7, where representative channels have been selected from maps in Fig. 3. We must remember the relatively

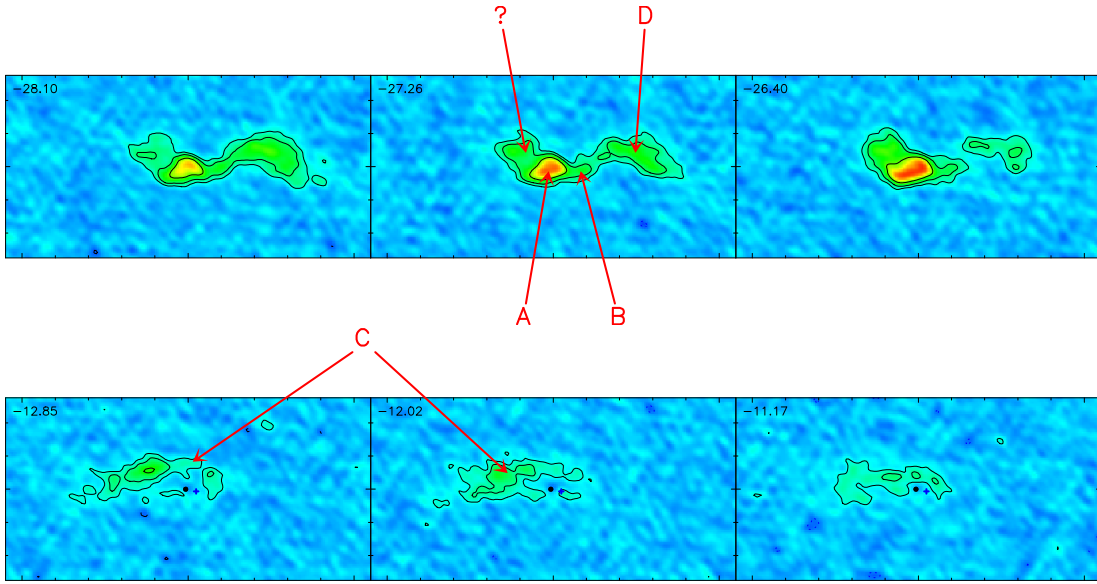


Figure 7: Correspondence between the different components of our simple model nebula and the main features of our maps. Some representative panels have been selected from Fig. 3.

high inclination of the orbital plane with respect to the plane of the sky, that its axis is more or less in the north-south direction, and, as mentioned, that the orbital apparent movement proceeds clockwise (Sects. 1, 3). The gas which is relatively going away from the observer (with relatively positive V_{lsr} , lower panels), must be represented in the model by the outer part of the first arm, **C**, its outward velocity component and the fact that it is placed behind the stellar system (according to the mentioned equator inclination) explain the observed positive velocities. The gas approaching us (relatively negative V_{lsr} , upper panels) comes from components **B** and **D**, whose clockwise rotation explains the observed negative velocity. It is necessary that both expansion and rotation appear in components **B**, **C**, and **D**.

Component **?** should be behind the stars (as **C**), in view of the positive declination offset, but its negative velocity would indicate that infall is the dominant kinematics. This component is not included for the moment in our model. Infall often appears in hydrodynamical simulations, particularly when the interaction is strong and very significantly distorts the originally expanding dynamics. The gas dynamics in some points will then be substituted by rotation and, if that rotation velocity is smaller than the Keplerian one, some of this material can come back to the AGB star.

We conclude that our simple model reasonably describes the main parameters of the CO-rich circumstellar gas. CO is only abundant in certain inner regions where molecules are protected from the WD UV flux. Those regions show, together with a central condensation, the spiral structure and equatorial focusing predicted by hydrodynamical models. The velocity of the extended components is always a combination of expansion and rotation. However, owing to the strong photodissociation effects, the distribution of the CO total abundance probably shows much higher contrasts than that of the total gas density.

Acknowledgments

This work has been supported by the Spanish MINECO, grant AYA2016-78994-P, and by the National Science Centre, Poland, grant OPUS 2017/27/B/ST9/01940.

References

- [1] Mohamed, S., & Podsiadlowski, P. 2012, *Baltic Astronomy*, 21, 88
- [2] de Val-Borro, M., Karovska, M., Sasselov, D. D., & Stone, J. M. 2017, *MNRAS*, 468, 3408
- [3] Saladino, M. I., Pols, O. R., & Abate, C. 2019, *A&A*, 626, A68
- [4] Gromadzki, M., & Mikołajewska, J. 2009, *A&A*, 495, 931
- [5] Bujarrabal, V., Mikołajewska, J., Alcolea, J., & Quintana-Lacaci, G. 2010, *A&A*, 516, A19
- [6] Bujarrabal, V., Mikołajewska, J., Alcolea, J., Castro-Carrizo, A., Ramstedt, S., 2016, *A&A*, 616, L3
- [7] Schmid, H. M., Bazzon, A., Milli, J., et al. 2017, *A&A*, 602, A53
- [8] Saberi, M., Vlemmings, W. H. T., & De Beck, E. 2019, *A&A*, 625, A81
- [9] Visser, R., van Dishoeck, E. F., & Black, J. H. 2009, *A&A*, 503, 323
- [10] Papoular, R. 2008, *MNRAS*, 390, 1727
- [11] Bujarrabal, V., Castro-Carrizo, A., Alcolea, J., et al. 2016, *A&A*, 593, A92

DISCUSSION

NOEL CASTRO SEGURA: Do you expect the wind accretion of this system to favor any kind of accretion geometry, i.e. column/disk/spherical(ish) accretion?

VALENTÍN BUJARRABAL: From the observational point of view, the emission of the WD surroundings shows a hint of elongated apparent shape, but not concluding at all. Observations and theory show, on the other hand, that accretion should take place mainly within the orbital plane and that the material approaching the WD must present a significant angular momentum excess, which strongly suggests the formation of an accretion disk. Calculations by Mohamed and Podsiadlowski (2012) and Chen et al. (2017) also confirm the formation of such disks, but, in any case, I am not an expert on these theoretical developments.

TIINA LIIMETS's Comment: Someone has to make a different model for the large-scale outside nebular features.